Available online at www.sciencedirect.com
SCIENCE DIRECT®
Bioorganic Chemistry 31 (2003) 172–190
BIOORGANIC CHEMISTRY
www.elsevier.com/locate/bioorg

De Novo design and utilization of photolabile caged substrates as probes of hydrogen tunneling with horse liver alcohol dehydrogenase at sub-zero temperatures: a cautionary note☆

Shiou-Chuan Tsai[a] and Judith P. Klinman[b,c,*]

[a] *Department of Chemical Engineering, Stanford University, California 94305, USA*
[b] *Department of Chemistry, University of California at Berkeley, CA 94720, USA*
[c] *Department of Molecular and Cell Biology, University of California at Berkeley, CA, 94720, USA*

Received 20 September 2002

Abstract

In order to understand the influence of protein dynamics on enzyme catalysis and hydrogen tunneling, the horse liver alcohol dehydrogenase (HLADH) catalyzed oxidation of benzyl alcohol was studied at sub-zero temperatures. Previous work showed that wild type HLADH has significant kinetic complexity down to −50 °C due to slow binding and loss of substrate [S.-C. Tsai, J.P. Klinman, Biochemistry, 40 (2001) 2303]. A strategy was therefore undertaken to reduce kinetic complexity at sub-zero temperatures, using a photolabile (caged) benzyl alcohol that prebinds to the enzyme and yields the active substrate upon photolysis. By computer modeling, a series of caged alcohols were designed de novo, synthesized, and characterized with regard to photolysis and binding properties. The *o*-nitrobenzyl ether **15**, with a unique long tail, was found to be most ideal. At sub-zero temperatures in 50% MeOH, a two-phase kinetic trace and a rate enhancement by the use of **15** were observed. Despite the elimination of substrate binding as a rate-limiting step, the use of caged benzyl alcohol does not produce a measurable H/D kinetic isotope effect. Unexpectedly, the observed fast phase corresponds to multiple enzyme turnovers, based on the stoichiometry of the substrate to enzyme. Possible side reactions and their effects, such as the re-oxidation of bound NADH and

☆ Supported by a grant (to JPK) from the National Science Foundation (MCB 9514126).
* Corresponding author. Fax: 1-510-643-6232/8369.
E-mail address: klinman@socrates.berkeley.edu (J.P. Klinman).

0045-2068/03/$ - see front matter
doi:10.1016/S0045-2068(03)00018-X

the dissipation of photo-excitation energy, may offer an explanation for the observed multiple-turnovers. The lack of observable deuterium isotope effects offers a cautionary note for the application of caged substrates to isolate and study chemical steps of enzyme reactions, particularly when NADH is involved in the reaction pathway.

1. Introduction

Extensive structural and functional studies have provided the foundation for our understanding of enzyme catalysis [1]. With the exception of protein conformational changes, the behavior of enzymes has been described largely within a static framework. However, there has been an increasing recognition of the importance of protein dynamics in enzyme catalysis, in particular, the contribution of protein vibrational modes to bond cleavage processes (cf. [2]).

Much of the experimental evidence for the link between protein motion and catalysis has come from studies of hydrogen transfer reactions [2–6]. Although hydrogen transfer reactions can, in principle, take place either by surmounting the reaction barrier semi-classically, or tunneling through the reaction barrier quantum-mechanically, the latter process has been found to be dominant in many enzyme catalyzed C–H cleavage reactions (cf. [7] and refs therein). Since hydrogen tunneling is highly dependent on the relative energies of reactant and product as well as the distance between donor and acceptor [2], modest changes in protein structure and dynamics can be expected to impact, to a significant extent, the degree of tunneling. Specifically, if the temperature is reduced to sub-zero, two opposing trends in hydrogen transfer may emerge: first, if protein dynamics impact the height and width of the reaction barrier, a reduction in protein motion that accompanies low temperature may lead to a reduction or loss of tunneling. On the other hand, very low temperatures will affect the Boltzmann distribution of molecules with sufficient energy to surmount the reaction barrier, such that the only option for chemical reaction may become barrier penetration [8,9].

In a previous study [9], using benzyl alcohol as the substrate to study both competitive and non-competitive KIEs, we observed hydrogen tunneling for a mutant form (F93W) of horse liver alcohol dehydrogenase (HLADH)[1] with little kinetic complexity down to −35 °C. At this temperature significant tunneling persisted, suggesting either that the tunneling-enhancing protein motions persisted at −35 °C or that barrier penetration through a more static barrier had begun to dominate the reaction coordinate. It was of great interest to reduce the experimental temperature below −35 °C to examine whether a transition between different types of tunneling

[1] *Abbreviations used*: HLADH, horse liver alcohol dehydrogenase; F93W, mutant HLADH that differs from the wild type enzyme by $Phe^{93} \rightarrow Trp$; YADH, yeast alcohol dehydrogenase; KIE, kinetic isotope effect; HPLC, high performance liquid chromatography; kDa, kilodalton; MeOH, methanol; BzOH, benzyl alcohol.

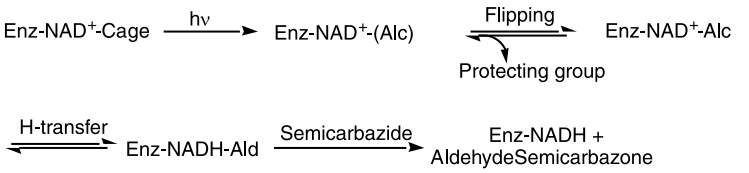

Scheme 1. Anticipated reaction pathway for interaction of HLADH with the caged reagent. Following photo-dissociation of the caged reagent, alcohol (Alc) is oriented to face the active site zinc. Flipping of bound alcohol is followed by the chemical (hydrogen transfer) step. Loss of bound aldehyde leads to its rapid trapping by excess semicarbazide, ensuring reaction irreversibility.

behavior could be detected, as was recently reported for a thermophilic ADH [8]. Because F93W HLADH is prone to precipitation below −35 °C, we turned to the study of the more stable wild type HLADH, which is active down to −50 °C. However, kinetic isotope effects with the wild type enzyme indicate significant kinetic complexity due to slow substrate binding/product release, which increases at lower temperatures and masks the observation of tunneling [9]. In order to study the behavior of HLADH below −35 °C, a new approach to reduce kinetic complexity was necessary.

Light-based deprotection of masked functional groups of certain biomolecules (''caged'' molecules) has been recognized as a simple, non-invasive technique to generate concentration gradients of substrates in a local environment [10]. Irradiation of the caged compounds with light removes the protecting group, with the subsequent generation of the substrate activity. Herein, we report a unique strategy to study hydrogen tunneling at sub-zero temperature, utilizing photolabile (caged) substrates of HLADH. As illustrated in Scheme 1, prebinding of caged substrate eliminates the kinetic complexity arising from slow substrate binding at sub-zero temperatures, as well as possible kinetic complexity arising from a more random binding mechanism for cofactor and substrate in the presence of cryosolvents [9]. An underlying assumption of Scheme 1 was that the overall photolysis reaction would be less thermally activated than subsequent chemistry [10], ensuring that the latter is kinetically dominant at reduced temperatures. Additionally, it was expected that reorientation of the photoreleased, bound substrate (Alc) would be rapid and facile. As we discuss herein, an optimal caged substrate (**15**) that binds tightly to HLADH was designed and synthesized. Detailed binding and kinetic studies indicate that this caged reagent introduces several levels of kinetic complexity that were not originally anticipated. This report offers a cautionary to the utilization of photolabile reagents to isolate chemical steps in enzyme reactions.

2. Materials and methods

Reagent grade benzyl alcohol and benzoic acid were obtained from Fisher. Prior to use, benzyl alcohol was purified by vacuum distillation. [Ring-^{14}C(U)]benzoic acid (ICN) had a specific activity of 56–65 Ci/mol. Liver alcohol dehydrogenase (HLADH) was obtained from Boehringer–Mannheim as a suspension in a 20 mM

potassium phosphate (pH 7.0) and 10% ethanol solution. NMR spectra were measured in $CDCl_3$ on either a Bruker 500 MHz or a Bruker 400 MHz NMR spectrophotometer.

Benzyl (2-nitrobenzyl) ether ***1*** *(Fig. 1B)*. To 1.0 g (6.62 mmol) of 2-nitrobenzyl alcohol in a 100-mL round-bottomed flask immersed in an ice-water bath was added 20 mL of dry THF followed by 320 mg (6.66 mmol) of powdered NaH (50% oil dispersion). After the gas evolusion subsided, 10 mL THF solution of benzyl bromide (1.10 g, 6.43 mmol) was added. After 20 h, the reaction mixture was quenched by the addition of 10 mL of water, followed by an extraction with ether (2×20 mL). The combined ether layer was washed with brine and then dried. Upon addition of *n*-pentane (10 mL), the unreacted starting material 2-nitrobenzyl alcohol (50 mg, 5%) precipitated and was collected by filtration. The filtrate was a colorless solution, which evaporated in air to give 0.54 g (25%) of compound **1** as white needles, m.p. 64–66 °C; ^{1}H NMR δ 8.05 (dd, $J = 8$, 1 Hz, 1H), 7.85 (dd, $J = 8$, 1 Hz, 1H), 7.63 (ddd, $J = 8$, 1, 1 Hz, 1H), 7.42 (ddd, $J = 8$, 1, 1 Hz, 1H), 7.40–7.29 (m, 5H), 4.95 (s, 2H), 4.66 (s, 2H); λ_{max} 290 nm ($\varepsilon = 4875\,cm^{-1}\,M^{-1}$); elemental analysis $C_{14}H_{13}NO_3$ calcd (%) C 79.53 H 6.20 N 6.63, found (%) C 78.89 H 6.25 N 7.00. Benzyl (2,4-dinitrobenzyl) ether **2** and benzyl (2-nitro-3,5-dimethoxybenzyl) ether **3** were attempted in a very similar fashion, but no products were obtained.

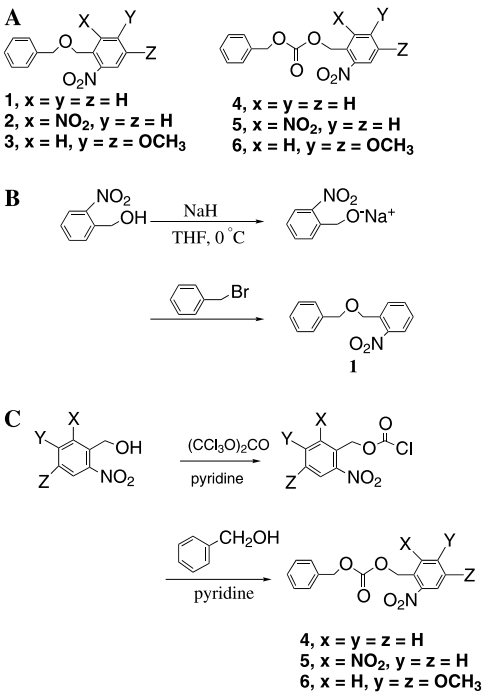

Fig. 1. (A) Structures of ether-linked (**1**–**3**) and carbonate-linked (**4**–**6**) substrates. (B) Synthesis of **1**. (C) Synthesis of **4**–**6**.

*Benzyl (2-nitrobenzyl) carbonate **4** (Fig. 1C)*. Into 15 mL dichloromethane solution of triphosgene (656 mg, 2.21 mmol) cooled to −80 °C, a 10 mL dichloromethane solution of dry pyridine (524 mg, 6.62 mmol) and 2-nitrobenzyl alcohol (1.0 g, 6.62 mmol) were added dropwise, and the reaction mixture was allowed to warm to room temperature and stirred overnight. The resulting yellow reaction mixture was then cooled to −80 °C, followed by the addition of a 10 mL dichloromethane solution of dry pyridine (524 mg, 6.62 mmol) and benzyl alcohol (716 mg, 6.62 mmol). The solution was then concentrated and washed with 10 mL dry THF, followed by filtration. Purification by column chromatography (silica gel packed with 30% benzene/*n*-hexane, eluted with 50% benzene/*n*-hexane) yielded 1.5 g (55%) of compound **4** as a white solid, m.p. 43–45 °C; ^{1}H NMR δ 8.12 (d, $J = 8$ Hz, 1H), 7.64 (d, $J = 1$ Hz, 1H), 7.63 (s, 1H), 7.62–7.45 (m, 1H), 7.39–7.33 (m, 5H), 5.60 (s, 2H), 5.20 (s, 2H); elemental analysis $C_{15}H_{13}NO_5$ calcd (%) C 62.71 H 4.56 N 4.87, found (%) C 62.39 H 4.54 N 4.79. Benzyl (2,4-dinitrobenzyl) carbonate **5** and benzyl (2-nitro-3,5-dimethoxybenzyl) carbonate **6** were synthesized in a similar fashion. **5**, m.p. 51–53 °C; ^{1}H NMR δ 8.06 (d, $J = 9$ Hz, 2H), 7.67 (t, $J = 8$ Hz, 1H), 7.34–7.30 (m, 5H), 5.61 (s, 2H), 5.11 (s, 2H); elemental analysis $C_{15}H_{12}N_2O_7$ calcd (%) C 54.27 H 3.64 N 8.44, found (%) C 54.44 H 3.65 N 8.60. **6**, m.p. 73–74 °C; ^{1}H NMR δ 7.71 (s, 1H), 7.38–7.34 (m, 5H), 6.70 (s, 1H), 5.59 (s, 2H), 5.20 (s, 2H), 3.93 (s, 3H), 3.85 (s, 2H); λ_{max} 342 nm ($\varepsilon = 3784\,cm^{-1}\,M^{-1}$); elemental analysis $C_{17}H_{17}NO_7$ calcd (%) C 58.79 H 4.94 N 4.03, found (%) C 59.01 H 4.85 N 3.95.

*3-Methoxy-4-(phenylmethoxy)benzaldehyde **7** (O-benzylvanillin) (Fig. 2A)*. A mixture of vanillin (20 g, 0.128 mol), benzyl bromide (22 g, 0.128 mol), potassium carbonate (8.8 g, 0.064 mol), and acetone (300 mL) were refluxed for 12 h and then were added to water (300 mL). The precipitated product recrystallized from ethanol to yield 31 g (100%) of compound **7** as colorless needles, m.p. 128–130 °C; ^{1}H NMR δ 9.81 (S, 1H), 7.43–7.23 (m, 8H), 5.22 (s, 2H), 3.92 (s, 3H); mass (M^+ n/z) 242.3.

*5-Methoxy-2-nitro-4-(phenylmethoxy)benzaldehyde **8** (O-benzyl-6-nitrovanillin)*. Powdered *O*-benzylvanillin (31 g, 0.128 mol) was added to nitric acid (150 mL; d 1.46) and stirred at 0 °C. After one hour the solid product was filtered and recrystallized from ethyl acetate to give 35 g (96%) of compound **8** as pale yellow needles, m.p. 212–214 °C; ^{1}H NMR δ 10.39 (s, 1H), 7.65 (s, 1H), 7.44–7.35 (m, 6H), 5.25 (s, 2H), 3.91 (s, 3H); mass (M^+ n/z) 287.3.

*4-Hydroxy-5-methoxy-2-nitrobenzaldehyde **9** (6-nitrovanillin)*. A mixture of pure *O*-benzyl-6-nitrovanillin (35 g, 0.123 mol) and acetic acid (240 mL) was kept at 85 °C while 48% hydrobromic acid (75 mL) was added. The reaction mixture was kept at 85 °C for 1 h. The solid product was filtered and recrystallized from hot ethanol to yield 14.5 g of compound **9** (60%) as yellow crystals, m.p. 208–210 °C; ^{1}H NMR δ 10.39 (s, 1H), 7.70 (s, 1H), 7.46 (s, 1H), 4.05 (s, 3H); mass (M^+ n/z) 197.1.

*4-(6′-Hydroxyhexoxy)-5-methoxy-2-nitrobenzaldehyde **10***. Compound **9** (5.0 g, 0.025 mol), KOH (1.425 g, 0.025 g) and 6-bromo-1-hexanol (4.6 g, 0.025 mol) were added with 50 mL dry ethanol and refluxed overnight. The reaction mixture was filtered, concentrated, extracted with ethyl acetate (2 × 250 mL), washed with water (2 × 200 mL) and brine, and then dried. Liquid chromatography (silica gel packed and eluted with 10% ethyl acetate/90% *n*-hexane) led to 2.5 g of compound **10**

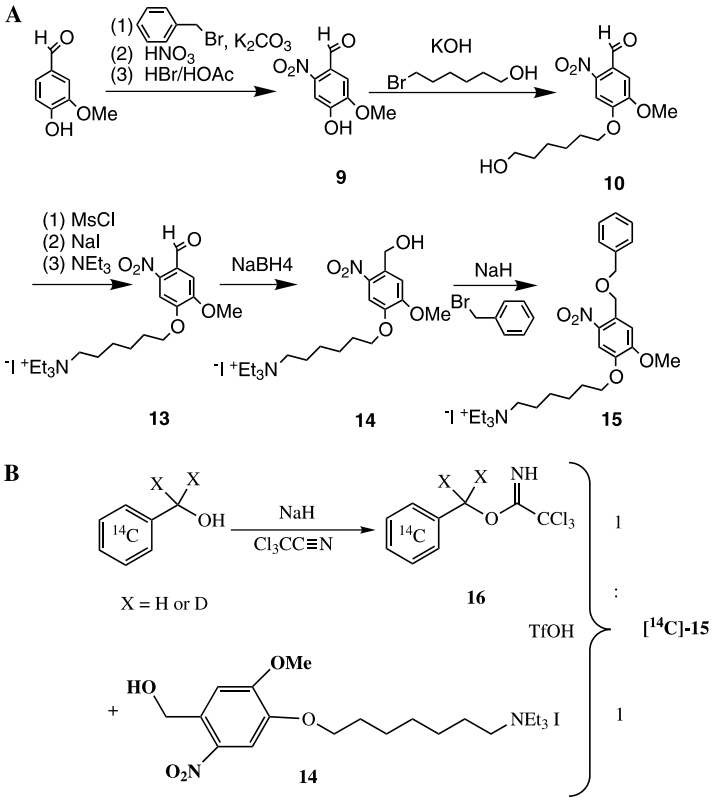

Fig. 2. (A) Reactions leading to the non-radioactive caged substrate **15**. (B) Reactions leading to the [^{14}C]-labeled protiated and deuterated caged substrate **15**.

(30%) as yellow oil, ^{1}H NMR δ 10.41 (s, 1H), 7.56 (s, 1H), 7.38 (s, 1H), 4.12 (t, $J = 7$ Hz, 2H), 3.97 (s, 3H), 3.64 (t, $J = 7$ Hz, 2H), 1.91–1.86 (m, 2H), 1.61–1.52 (m, 2H), 1.50–1.41 (m, 4H); mass (M^+ n/z) 297.3.

4-[6′-(Methanesulfonyl)hexoxy]-5-methoxy-2-nitrobenzaldehyde ***11***. Compound **10** (2.5 g, 0.008 mol) and triethylamine (3.5 mL, d 0.726, 0.025 mol) were dissolved in 100 mL dichloromethane under dry nitrogen, and mesityl chloride (1.6 mL, d 1.48, 0.021 mol) was added by syringe. The reaction mixture was refluxed for 4 h, extracted with water (100 mL × 2), washed by brine, and then dried. Upon concentration yielded 3.24 g of compound **11** (100%) as yellow oil, ^{1}H NMR δ 10.42 (s, 1H), 7.57 (s, 1H), 7.39 (s, 1H), 4.24 (t, $J = 7$ Hz, 2H), 4.13(t, $J = 7$ Hz, 2H), 3.99 (s, 3H), 2.99 (s, 3H), 1.92–1.88 (m, 2H), 1.80–1.77 (m, 2H), 1.52–1.51 (m, 4H); mass (M^+ n/z) 375.4.

4-(6′-Iodohexoxy)-5-methoxy-2-nitrobenzaldehyde ***12***. Compound **11** (3.24 g, 8.5 mmol) was dissolved in acetone 120 mL, and sodium iodide (3.7 g, 25 mmol) was added. The clear yellow solution was refluxed overnight, followed by filtration and concentration to yield 3.61 g of compound **12** (100%) as an orange solid, m.p.

68–70 °C; ^{1}H NMR δ 10.42 (s, 1H), 7.57 (s, 1H), 7.39 (s, 1H), 4.13 (t, $J = 6$ Hz, 2H), 3.98 (s, 3H), 3.18 (t, $J = 7$ Hz, 2H), 1.90–1.83 (m, 4H), 1.54–1.48 (m, 4H); mass (M^+ n/z) 412.3.

6-(4′-Formyl-2′-methoxy-5′-nitrophenoxy)hexyl triethylammonium iodide ***13***. Compound **12** (3.6 g, 8.5 mmol) was dissolved in 50 mL acetonitrile, and 30 mL triethylamine was added dropwise. The reaction mixture turned from orange to yellow, and was refluxed for 4 h, followed by concentration and washing with ether (3×200 mL) to yield 3.66 g of compound **13** (90%) as yellow oil, ^{1}H NMR δ 10.43 (s, 1H), 7.60 (s, 1H), 7.40 (s, 1H), 4.17 (t, $J = 6$ Hz, 2H), 4.01 (s, 3H), 3.50 (q, $J = 7$ Hz, 6H), 3.38–3.34 (m, 2H), 2.01–1.94 (m, 2H), 1.81–1.65 (m, 2H), 1.45–1.39 (m, 4H), 1.21 (t, $J = 7$ Hz, 9H); mass (M^+ n/z) 381.5.

6-[4′-(Hydroxymethyl)-2′-methoxy-5′-nitrophenoxy]hexyl triethylammonium iodide ***14***. Compound **13** (3.6 g, 7 mmol) was dissolved with 50 mL dry methanol under dry nitrogen, and added to 50 mL stirred ice-cold methanol solution of sodium borohydride (0.16 g, 4.3 mmol). The reaction was stirred at 0 °C for one hour. Acetone (100 mL) was added to the resulting solid, followed by filtration and concentration to yield 3.66 g of compound **14** (100%) as light yellow oil, ^{1}H NMR δ 7.57 (s, 1H), 7.39 (s, 1H), 5.05 (s, 2H), 4.25 (t, $J = 6$ Hz, 2H), 3.95 (s, 3H), 3.50 (q, $J = 7$ Hz, 6H), 3.39–3.34 (m, 2H), 1.90–1.70 (m, 2H), 1.80–1.55 (m, 6H), 1.21 (t, $J = 7$ Hz, 9H); mass (M^+ n/z) 383.5.

6-{2′-Methoxy-5′-nitro-4′-[(phenylmethoxy)methyl]phenoxy}hexyltriethylammonium iodide ***15*** *(Fig. 2A)*. Compound **14** (0.5 g, 1 mmol) and benzyl bromide (5 mL, d 1.4, largely in excess) were added via syringe to 10 mL dry THF, followed by the addition of sodium hydride (0.036 g, 1.5 mmol) and was refluxed overnight. The reaction mixture was then quenched by the addition 100 μL MeOH, followed by filtration and concentration to yield compound **15** (0.6 g, 100%) as yellow oil, ^{1}H NMR δ 7.65 (s, 1H), 7.45–7.30 (m, 6H), 4.95 (s, 2H), 4.67 (s, 2H), 4.18 (t, $J = 6$ Hz, 2H), 3.88 (s, 3H), 3.39 (q, $J = 7$ Hz, 6H), 3.19–3.08 (m, 2H), 1.85–1.80 (m, 2H), 1.75–1.65 (m, 2H), 1.65–1.50 (m, 2H), 1.50–1.40 (m, 2H), 1.29 (t, $J = 7$ Hz, 9H); λ_{max} 355 nm ($\varepsilon = 3500\,cm^{-1}\,M^{-1}$); mass ($M^+$ n/z) 473.6. The overall yield from vanillin to compound **15** is 15%.

[Ring-^{14}C(U)]benzyl alcohol. Lithium aluminum hydride 30 mg (1 mmol) was added to a stirred dry ether solution (5 mL) under nitrogen. One mCi of [ring-^{14}C(U)]benzoic acid (0.015 mmol, 65 mCi/mmol) in 1 mL toluene was added and stirred for 4 h. The reaction mixture was quenched by adding 1 mL of ice water, followed by the addition of 2 mL HCl to dissolve the resulting aluminum hydroxide. The aqueous layer was extracted with ether (5 mL × 4), and the combined ether layer was washed with brine and then dried over $MgSO_4$. Concentration in vacuo yielded [ring-^{14}C(U)]benzyl alcohol (950 μCi, yield 95%). The crude product can be further purified by HPLC, eluting at 14 min on a reverse phase Rainin C18 column (25 cm long, 100 Å pore, 5 mm o.d.). An isocratic solvent was used (12% CH_3OH, 12% CH_3CN, and 76% water), at a flow rate of 1 ml/min. Since no ring modification took place and no non-radioactive starting material was introduced during the synthesis, it was assumed that the specific activity of the product is close to the starting material (65 Ci/mol).

[1,1-$^2H_2$]-[ring-^{14}C(U)]benzyl alcohol. This was obtained quantitatively according to the above procedure, except that a batch of [ring-^{14}C(U)]benzoic acid with a specific activity of 56 Ci/mol was used. Since no ring modification took place and no non-radioactive starting material was introduced during the synthesis, it was assumed that the specific activity of the product is close to the starting material (56 Ci/mol).

[Ring-^{14}C(U)]benzyl trichloroacetimidate **16**. [Ring-^{14}C(U)]benzyl alcohol (100 μCi, 65 Ci/mol, 1.5 μmol) and 1 mL of dry ether stirred while sodium hydride (1 mg, 41.6 μmol) was added. After 10 min, dry trichloroacetonitrile (1.4 mg, 9.25 μmol) was added to the reaction mixture. After 4 h, the reaction mixture was quenched with 10 μL of MeOH and concentrated, followed by washing with 4×2.5 mL of dry *n*-pentane. The solution was washed with 2×1 mL of MeCN/water (65/35), followed by brine and then dried. Upon removal of *n*-pentane by vacuum, the product **16** was obtained quantitatively as a colorless liquid. Compound **16** could be further purified by passing through a 10 cm glass column (packed with silica gel in 5% EtOAc/*n*-hexane, eluted with 5% EtOAc/*n*-hexane) or by HPLC (condition described above); yield 80–90%. Since no ring modification took place and no non-radioactive starting material was introduced during the synthesis, it was assumed that the specific activity of the product is close to the starting material (65 Ci/mol).

[Ring-^{14}C(U)]-1,1-$^2H_2$-benzyl trichloroacetimidate. This was obtained according to a similar procedure except that [Ring-^{14}C(U)]-1,1-$^2H_2$-benzyl alcohol was used; yield 80–90%. Since no ring modification took place and no non-radioactive starting material was introduced during the synthesis, it was assumed that the specific activity of the product is close to the starting material (56 Ci/mol).

[Ring-^{14}C(U)]-caged substrate **15** *(Fig. 2B)*. To exchange the anion from iodide to ClO_4^-, a solution of compound **14** (5 mg in 1 mL pure water) was passed through a C18 sep-pak column (pre-washed with 2×10 mL MeCN, 2×10 mL water, and 3×10 mL 0.1 M $NaClO_4$ methanol solution) and eluted with 1 mL 0.1 M $NaClO_4$ methanol solution. Upon concentration, the ClO_4^- salt of **14** was obtained quantitatively. A dry dichloromethane solution of the ClO_4^- salt of **14** (1 mg, 2.07 mmol), non-radioactive benzyl trichloroacetimidate (0.52 mg, 2.06 mmol) and [ring-^{14}C(U)]benzyl trichloroacetimidate **16** (100 μCi, 1.5 μmol) was added. The final total volume was 1.5 mL. The reaction was initiated by the addition of triflic acid (0.01 g, 0.05 mmol). The reaction mixture was neutralized by the addition of powdered sodium bicarbonate, followed by filtration and concentration to yield product (1 mg, 95%) as a yellow liquid. The product can be further purified on HPLC by elution on a C-18 column with 0.1 M sodium cacodylate (pH 7.0) buffer in MeCN/Water (65/35) and is eluted at 12 min. The concentration of **15** is determined by the extinction coefficient of **15** at λ_{max} 355 nm ($\varepsilon = 3500\ cm^{-1}M^{-1}$). Final specific activity of **15**, based on the radiation count (in dpm) in a sample with known concentration, was 54 mCi/mol.

[Ring-^{14}C(U)]-1,1-$^2H_2$-caged substrate **15**. This was obtained according to a similar procedure, except that [ring-^{14}C(U)]-1,1-$^2H_2$-benzyl trichloroacetimidate was used; yield 85–95%. Final specific activity was 45 mCi/mol.

2.1. Computer modeling

The coordinate file of the X-ray crystal structure of the productive ternary complex HLADH-NAD^+-*p*-bromobenzyl alcohol was obtained from the laboratory of Prof. B. Plapp [11]. Computer modeling was performed on a Silicon graphics Indigo computer with InsightII software. The caged substrates were docked visually by constraining the distance between the substrate and the enzyme residues to be greater than the sums of van der Waals radii of the corresponding atoms. Fittings of the caged substrates into the binding pocket were achieved by the overlapping of the benzene ring of the caged substrates with the benzene ring of *p*-bromobenzyl alcohol in the ternary complex structure, followed by bond-twisting around the two benzylic CH_2 group in the caged substrates to avoid any steric interaction. Benzyl alcohol flipping was visualized first by overlapping the benzene ring of benzyl alcohol with *p*-bromo benzyl alcohol in the original PDB file, followed by a rotation of the benzyl alcohol around the center of the benzene ring.

2.2. Photolysis of the caged substrates

A quartz cuvet (1 mm light path) was purged with dry nitrogen and thermostated by a cell holder with a circulation jacket. Into a quartz cuvet was injected 150 μL solution of compound **1**, **6**, or **15** (ca. 0.34 mM) via a syringe. The irradiation of compound **1**, **6**, or **15** was carried out by an Nd YAG Laser at 355 nm. The photo-cleavage reaction was monitored by a Hewlett–Packard photo diode array spectrometer and ^1H NMR. A decrease in the concentration of the caged substrate was measured by the decrease of their UV/Vis absorptions. The absorption wavelength and extinction coefficient for **1**, **6**, and **15** are 290 nm ($\varepsilon = 4875\,cm^{-1}M^{-1}$), 342 nm ($\varepsilon = 3784\,cm^{-1}M^{-1}$), and 355 nm ($\varepsilon = 3500\,cm^{-1}M^{-1}$), respectively. This can be plotted against time and fitted with first order kinetics to obtain a photolysis rate for each of the caged substrates. Quantum yield was measured by chemical actinometry, with a standard photolysis of $K_3Fe(C_2O_4)_3$ (quantum yield $f_{297} = 1.24$, $f_{358} = 1.25$) [10]. The photolysis rates for both the caged substrates and $K_3Fe(C_2O_4)_3$ were measured under identical conditions. The quantum yields of the caged substrates were calculated according to reference [10]:

$$\phi_{cage} = \phi_{Fe} \times \frac{v_{cage}}{v_{Fe}}, \tag{1}$$

where ϕ_{cage} is the quantum yield for the photolysis of the caged substrates, ϕ_{Fe} is the quantum yield for the photolysis of $K_3Fe(C_2O_4)_3$, v_{cage} is the photolysis rate for the caged substrates, and v_{Fe} is the photolysis rate for $K_3Fe(C_2O_4)_3$ [5]. It was found that the quantum yield of **15** is 0.24.

Binding study of the caged substrates. A CARY-118b UV/Vis spectrophotometer was modified to work at sub-zero temperatures, as mentioned in previous work [9]. The binding kinetics was measured as described previously [9].

2.3. Design of low-temperature photolysis chamber

A chamber was constructed of polyacrylate plastic, which is not only a good thermo-insulator but also lightweight and transparent. A round quartz cuvet (1 mm light path) was installed in the chamber, as well as a thermostated cuvet holder matching the size and shape of the cuvet. The thermostated jacket of the cuvet holder was attached to the inlet and outlet of a Neslab ULT-80 cryogenic bath by two C-Flex tubings. Two round quartz windows (2 in. o.d.) were installed on either side of the chamber to define the light path for the YAG laser beam (5 ns pulse, average power 150 mW, 355 nm). The temperature in the cuvet was constantly monitored by a Fisher thermocouple with a type K probe (0.4 mm o.d.). To prevent moisture condensation on the cuvet, a stream of cold, dry nitrogen was blown into the bottom of the cuvet holder via a C-Flex tubing, creating a dry nitrogen jacket around the cuvet. The cold, dry nitrogen was cooled by passing through a homemade copper coil (15 cm diameter, 100 turns). To prevent moisture condensation on the quartz windows of the chamber, two separate streams of room temperature, dry nitrogen were blown directly on the two quartz windows. The low-temperature chamber can be operated within a very stable temperature range down to −70 °C.

2.4. Photolysis of **15** pre-bound to HLADH

One hundred and fifty microliters of the sample, containing 20 μM HLADH, 1 mM of ^{14}C-labeled protiated or deuterated **15** (concentration determined by the extinction coefficient at 355 nm) and 10 mM of NAD, were placed into the cuvet. The buffer contained 100 mM sodium cacodylate and 200 mM semicarbazide (pH* 7.0 [9]) in 30–50% MeOH. The sample was then irradiated with the YAG Laser in full power for 0–15 s. The reaction for the photolysis of **15** was initiated by laser irradiation. A control of 20 μM HLADH and 10 mM NAD were added to the cuvet at a stable temperature, followed by the initiation of the reaction by the addition of 1 mM ^{14}C-labeled benzyl alcohol (freshly distilled one day prior to the experiment) with a pipetteman (both benzyl alcohol and the pipette tip were pre-equilibrated at the same temperature as that in the cuvet) and simultaneous laser irradiation for 0–300 s. Each sample (150 μL) contained 15,000–18,000 dpm of ^{14}C-labeled **15** or benzyl alcohol. Reactions of either **15** or benzyl alcohol were rapidly quenched with 20 μL of 2 mM $HgCl_2$, using a pre-chilled pipette tip to mix the solution. The time points at 5, 10, and 15 s were conducted with varying laser irradiation time at 5, 10, and 15 s, and the reaction was quenched with mercury salt immediately after laser irradiation, while the time point at 30, 60, and 300 s was irradiated for 15 s and quenched thereafter. Quenched samples were retrieved from the cuvet and frozen in dry ice. Upon thawing for analysis, samples were centrifuged, injected to an HPLC column (25 cm long, 100 Å pore), and eluted at 1 mL/min by either a Beckman 110B or a Shimatsu 10-SV HPLC system. The HPLC program was set to elute the sample isocratically (12:12:76, v/v, MeCN:MeOH:water) for 30 min, followed by a 10 min gradient to 100% MeOH and 0.1 M $NaClO_4$. The absorption of at least one wavelength (210, 280, or 350 nm) was monitored during the HPLC run. The eluant was collected with

a LKB-Bromma 2112 Redirac fractional collector in fractions of 1.5 mL in 20 mL plastic vials; 12 mL of scintillation liquid (Ecolite from ACN) was then added to each vial. The vials were counted on a LKB-Wallac 1209 Rackbeta liquid scintillation counter for 300 s with 15 s of internal standard counting. Benzyl alcohol, benzaldehyde semicarbazone, and the caged substrate **15** eluted at 14–15, 28–31, and 40–45 min, respectively. The percentage of conversion was calculated for each time point by the ratio of radioactivity between the product benzaldehyde semicarbazone and total counts in the sample. The time traces were plotted for percentage of conversion versus time (Fig. 3).

Control experiments were conducted and analyzed similar to the above reaction condition. A control zero-time point was taken prior to the laser irradiation of **15** and analyzed as above; benzyl alcohol or its enzymatic products were not found in these zero-time point samples. Also, during photolysis, temperatures were monitored by a thermocouple, indicating no increase in temperatures. Further, to monitor laser damage to the enzyme HLADH, a 150 μL sample of 20 μM HLADH and 10 mM NAD, with or without 1 mM non-radioactive **15**, was irradiated with laser for 60 s. The enzyme activity is then analyzed as previously described [12]. HLADH was found to retain full activity after laser irradiation, indicating no photo-damage to the enzyme plus NAD. Additionally, 1 mM of benzyl alcohol was laser-irradiated for 60 s in the presence of 10 mM NAD. This is followed by the addition of enzyme HLADH to monitor the initial rate of NADH formation [12]. The observed initial rate is similar to the control without laser irradiation, indicating no photo-damage to benzyl alcohol and NAD upon laser irradiation. Photolysis of 1 mM NADH in the presence of 1 mM **15** was analyzed by the decrease of the absorbance at 340 nm (λ_{max} of NADH). Finally, photolysis of **15** in the presence of buffer and 10 mM NAD produced only benzyl alcohol as analyzed by HPLC.

3. Results and discussion

3.1. Design principles

A number of important design principles of the caged substrate are related to its binding affinity and orientation within HLADH. The X-ray crystal structure of HLADH reveals that the residues in the binding pocket of HLADH are highly hydrophobic [11], such that incorporation of a hydrophobic component was expected to lead to strong binding of caged substrates to the binding pocket. However, a simple hydrophobic caged substrate might bind to the enzyme in non-productive modes, with the alcohol precursor pointing toward solvent rather than to the cofactor. Constraints were needed to ensure that the caged substrate would reside in a productive binding mode that upon photolysis releases alcohol at the bottom of the cleft leading to the active site. As will be obvious from the structures of caged reagents described below, photo-released alcohol is required to flip by ca. 180° in order to orient the alcohol functional group in a position suitable for catalysis (cf. Schemes 1 and 2). Computer modeling indicated that there was sufficient space for this flipping to occur

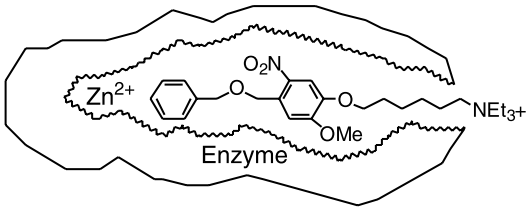

Scheme 2. Illustration of the expected orientation of the final caged reagent (**15**) within the active site of HLADH. The quaternary amine both increases the solubility of the caged reagent and places the alcohol precursor near the active site of enzyme.

without significant steric interactions. One final constraint was that the caged substrate have a significant UV/Vis absorption at a wavelength greater than 300 nm, to place its λ_{max} away from the range of protein absorbance.

*3.2. Synthesis and properties of caged substrates **1–6***

The simplest compound (**1** in Fig. 1A), contains the 2-nitrobenzyl moiety and the substrate moiety. Initially, we attempted to synthesize **1** by the deprotonation of benzyl alcohol, followed by its nucleophilic attack on 2-nitrobenzyl bromide. This reaction did not produce **1**, possibly due to the deprotonation of 2-nitrobenzyl bromide to yield a resonance stabilized anion intermediate. It was found that reversing the polarity of the components (deprotonation of 2-nitrobenzyl alcohol followed by coupling with benzyl bromide) gave the desired cage compound **1** (Fig. 1B).

The UV/Vis absorption spectrum of **1** shows the $\pi \rightarrow \pi^*$ absorption [7] at 295 nm ($\varepsilon = 4875\,cm^{-1}M^{-1}$). The $n \rightarrow \pi^*$ transition is hidden within this absorption and is the main excitation mode that results in the photo-cleavage reaction [13]. As mentioned above, a compound with absorption above 300 nm was preferred to allow for optimal photo-cleavage with minimal photo-damage of the protein. Different functional groups were therefore added to **1** to generate **2** and **3**; additionally, a series of compounds using carbonate as the leaving group (**4–6**) was synthesized. The latter were obtained by the use of a stoichiometric amount of triphosgene [14] instead of phosgene gas (Fig. 1C). Triphosgene has not been previously applied to the synthesis of a mixed carbonate.

Among these caged substrates, **6** showed a significant $n \rightarrow \pi^*$ transition at 342 nm. The photolysis of **6** by a YAG laser (355 nm) was completed in 10 s. However, the highest concentration of **6** that could be dissolved in 30% methanol/water at 3 °C was found to be 25 μM. This can be compared to a $K_i \approx 75\,\mu M$, determined for **6** in 30% MeOH at 0 °C. It was clear that a re-designed compound was needed with increased solubility in relation to its dissociation constant.

3.3. A long-tailed caged substrate

To increase solubility while retaining the desirable features of **6**, a caged substrate was designed to contain a long hydrophobic tail with an ionic end. The

length of the hydrophobic tail was selected based on computer modeling; a six carbon chain provides just enough length for the ionic group to protrude out of the substrate binding pocket and into the bulk solvent (Scheme 2). The ionic tetra-alkyl ammonium group provides better solubility, while the hydrophobic tail increases the binding of the caged substrate within the hydrophobic substrate-binding pocket. Moreover, charge repulsion between the positively charged end of the caged reagent and the positively charged zinc ion in the enzyme active site, as well as steric hindrance from the bulky tetra-alkyl ammonium group, was expected to greatly favor a productive binding mode. We believe this is the first time that a caged substrate has been selectively modified for a specific enzyme active site.

The synthesis of **15** (Figs. 2A and B) began with commercially available vanillin, which was protected as a benzyl ether (**7** in Section 2) via a Williamson synthesis, followed by a nitration at the 6-position (**8** in Section 2) and a deprotection to remove the benzyl group that produces 6-nitrovanillin, **9**. The attachment of a hydrophobic tail to **9** by a second Williamson synthesis was, however, problematic. Compound **10** was eventually obtained by the deprotonation of compound **9** with dry KOH, followed by coupling with a stoichiometric amount of dry 6-bromo-1-hexanol. The alcohol functional group in compound **10** was activated with mesyl chloride to yield the mesylate (**11** in Section 2). This reacted easily with sodium iodide to form the iodide (**12** in Section 2), followed by reaction with triethylamine to generate **13**. Reduction of the aldehyde to the alcohol (**14**), deprotonation with NaH and reaction with an excess amount of benzyl bromide in THF produced the caged substrate **15**. Compound **15** is stable in aqueous solution and is not easily photolyzable by daylight. For the synthesis of radiolabeled **15**, the final coupling step for the ether formation became a problem. Due to the change of reaction scale, a coupling between [^{14}C]-labeled benzyl bromide and compound **14** failed to produce radiolabeled **15**. Many different reactions were attempted unsuccessfully, including reaction of [^{14}C]-labeled benzyl bromide with a silver salt prior to coupling with **14** [15], as well as a Mitsunobu reaction that coupled **14** with [^{14}C]-labeled benzyl alcohol by reactions with triphenyl phosphine and diethylacetadiimide (DEAD) [16]. Eventually, the [^{14}C]-labeled **15** was synthesized by an acid-catalyzed coupling (trifluoroacetic acid, TfOH) between a stoichiometric amount of the ClO_4 salt of **14** and [^{14}C]-labeled benzyl trichloroacetimidate **16** (Fig. 2B) [17].

The photolysis rate of **15** is solvent independent in water, methanol, acetonitrile, or mixtures of these solvents. **15** were completely photolyzed to benzyl alcohol in 60 s of laser irradiation at room temperature. The tetra-alkyl ammonium tail end of **15** greatly increases its solubility, which exceeds 10 mM. The ability of **15** to bind to HLADH was assayed by a steady-state inhibition study, showing that **15** is a competitive inhibitor of the substrate benzyl alcohol in 30% and 50% MeOH, with a K_i of 75 μM in 30% MeOH at 3 °C (Table 1). The increasing concentration of MeOH increases both the K_M of benzyl alcohol and the K_i of **15**. We note that value of K_i, relative to K_M, goes down somewhat as the percentage of the cryosolvent increases (Table 1).

Table 1
Interactions of HLADH with benzyl alcohol and **15** in the presence of increasing MeOH[a]

Solvent	k_{cat} (s^{-1})	K_M(BzOH) (μM)	K_i(cage) (μM)	K_i/K_M
30% MeOH	0.65	110	75	0.68
50% MeOH	0.024	1500	630	0.44
60% MeOH	0.027	1600	880	0.55
70% MeOH	0.021	2100	1100	0.54

[a] All experiments were carried out in a 100 mM cacodylate, 200 mM semicarbazide, and 10 mM NAD buffer (pH* 7.0) at 3 °C.

*3.4. Rate enhancement for product formation from caged substrate **15** at 0 °C*

An excess of [^{14}**C**]-labeled **15** or [^{14}C]-labeled benzyl alcohol (as the control) was incubated with HLADH and NAD^+; the mixture was then photolyzed with increasing irradiation time periods in 50% MeOH at 0 °C (Fig. 3A). Over the time course, the percent of photolysis proceeds to completion (Fig. 3A, ×—×). The time points at 5, 10, and 15 s were conducted with varying laser irradiation time (for 5, 10, and 15 s) and the reaction was quenched with mercury salt immediately after laser irradiation, while the time points at 30, 60, and 300 s were irradiated for 15 s and quenched at the appropriate time. The radiolabel ensured a sensitive measurement of the concentration of **15**, benzyl alcohol and the benzaldehyde product. A two-phase kinetic trace was observed with **15** pre-bound to HLADH (Fig. 3A, ●—●). It appears that in the slow phase, the photolyzed **15** reacts with a similar rate as the oxidation of free benzyl alcohol (Fig. 3A, ■—■), suggesting that after 30 s, photolyzed **15** (i.e., benzyl alcohol) reacts from the solution and behaves like free benzyl alcohol. However, in the fast phase before 30 s, photolyzed **15** creates a burst of product formation, resulting in a much faster rate than that of free benzyl alcohol oxidation. From the observed rate acceleration, it appeared that the prebinding of **15** eliminated the kinetic complexity of binding at 0 °C. We proceeded to conduct the same experiment at subzero temperatures.

3.5. Lack of H/D KIE at −30 °C

At −30 °C, the photolysis proceeded to 80% completion (Fig. 3B, ×—×). A two-phase kinetic trace was again observed upon photolysis of **15** (1 mM) in the presence of HLADH (20 μM) and NAD (10 mM) in 50% MeOH. Either 1 mM of [^{14}C]-labeled protiated (Fig. 3B, ●—●) or deuterated **15** (Fig. 3B, △—△) was used for the measurement of non-competitive kinetic isotope effects. As shown, the percent conversion is much higher for the reaction of pre-bound **15** than the oxidation of benzyl alcohol (Fig. 3B, ■—■). Similar to the finding at 0 °C, the observation of rate acceleration by **15** seemed to indicate that **15** had bound to HLADH prior to the photolysis and that the kinetic complexity from substrate binding was eliminated by the use of the cage strategy. The rate of photolysis of **15** approximates the rate of oxidation of the pre-bound substrate, resulting in 50% photolysis of **15** in 5–10 s. Most significantly, the time traces of protiated and deuterated **15** are very similar, with the

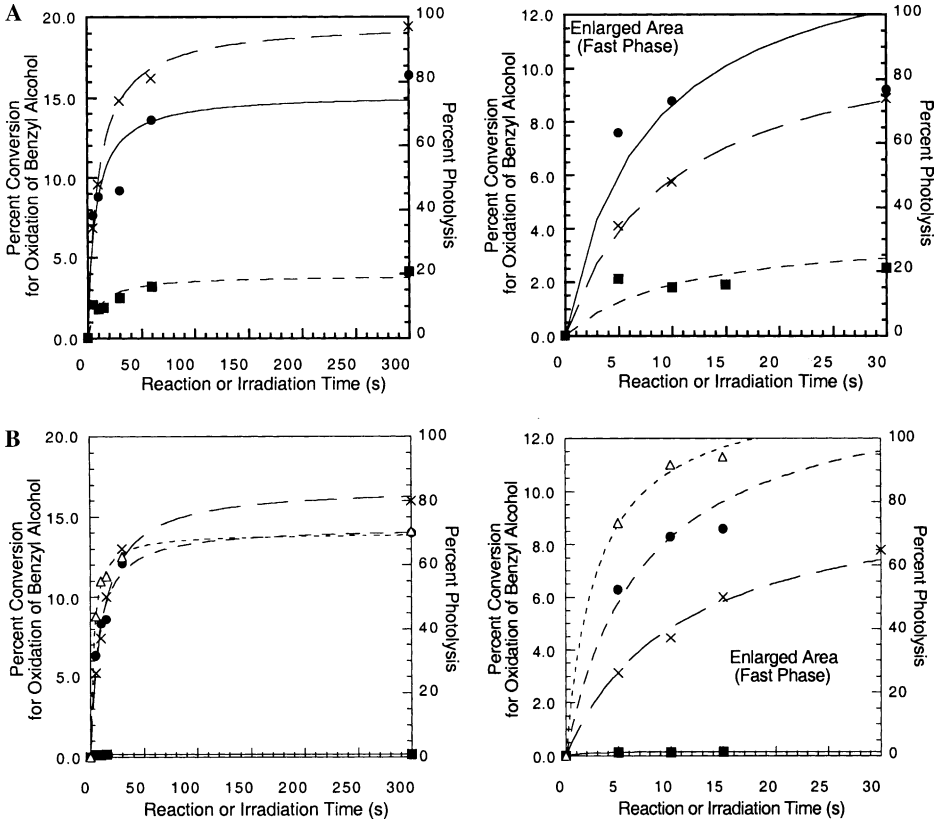

Fig. 3. (A) Photolysis of [^{14}**C**]-**15** or [^{14}**C**]benzyl alcohol with HLADH at 0 °C in 50% MeOH. (●) % of BzOH oxidation from **15**; (■) % of BzOH oxidation from free BzOH; (×) % of photolysis of **15**. (B) Photolysis of protiated or deuterated [^{14}**C**]-**15** at −30 °C in 50% MeOH. (●) % of BzOH oxidation from protiated **15**; (△) % of BzOH oxidation from the deuterated **15**; (■) % of BzOH oxidation from free BzOH; (×) % of **15** photolysis in a separate experiment from above. The similarity in the time trace between protiated and deuterated [^{14}**C**]-**15** indicates a lack of non-competitive H/D KIE. For both (A) and (B), all experiments were conducted in 150 μL of 200 mM semicarbazide and 100 mM sodium cacodylate (pH 7.0) 50% MeOH buffer with 20 μM HLADH, 10 mM NAD and 1 mM **15** or BzOH. The samples were irradiated for 15 s, except for the samples that were quenched before 15 s, which were irradiated for the same amount of time as the reaction.

deuterated substrate showing a slightly higher percent conversion than that of the protiated substrate in the fast phase. In comparison, our previous study of non-competitive H/D KIE at −30 °C, using protiated and deuterated benzyl alcohol to measure steady-state parameters, gave a $^{D}(k_{cat}/K_{M})$ of 2.7 for the wild type enzyme and $^{D}(k_{cat}/K_{M})$ of 6.0 for the F93W mutant [4]. If the fast phase is, as anticipated, a single-turnover event that isolates the hydrogen-transfer step as the major rate limiting step, the non-competitive H/D KIE in the fast phase should be higher than the value of ca. one measured in steady state, i.e., at each time point during the fast phase, the

protiated **15** should show a percent conversion at least 2.7 times higher than that of the deuterated substrate. The similarity of the time traces between protiated and deuterated **15** indicates that steps other than the hydrogen transfer step have become rate limiting in the reaction utilizing the caged substrate **15**. Since the photolysis reaction (Fig. 3B, ×—×) appears to react on a comparable timescale as the enzymatic conversion (Fig. 3B, ●—●), it was possible that the turnover rate for bound **15** was dictated by the photolysis reaction. This would have explained not only the lack of an H/D KIE but also the absence of a significant temperature dependence of the time traces (compare the percentage of conversion in Figs. 3A and B), since a photo-activated process is less temperature-dependent than a thermally-activated one [10].

3.6. Analysis of events during the fast phase

Further complication arises, however, from the results of Fig. 3B when we consider the stoichiometry of **15** versus HLADH. It can be estimated that under the condition of 20 μM of HLADH and 1 mM of **15** (with a K_i of 1 mM in 50% MeOH), ca. 10 μM of **15** will prebind to HLADH. Upon photolysis, a maximum concentration of 10 μM of pre-bound benzyl alcohol is expected to be converted to benzaldehyde in a single enzyme turnover; therefore, the maximum percentage of conversion upon photolysis of **15** for a single enzyme turnover should be 10 μM/1 mM = 1%. Even if the binding constant (K_i) were much smaller than 1 mM, such that a near-stoichiometric binding between HLADH and **15** had occurred, the maximum conversion would only be 20 μM/1 mM = 2%. However, the fast phase shows a burst of >10% conversion, which indicates multiple enzyme turnovers in the fast phase.

What can be the explanation for the observed multiple-turnovers in the first phase, and is this related to an H/D KIE close to unity? First, extensive control experiments eliminate a number of possible errors in the observations: (i) the concentration of pure **15** (1 mM) was determined by its extinction coefficient immediately before the experiments and should be accurate; (ii) a zero-time point was taken to ensure that no **15** had photolyzed prior to laser irradiation; (iii) the amount of radioactivity was kept constant (15,000–18,000 dpm) among samples; (iv) the total amount of radioactivity post photolysis from HPLC fractions is consistent with the amount prior to laser irradiation; and (v) the temperature of the photolysis cell, monitored with a thermo-couple, did not increase during or after photolysis. We can rule out any rate limiting step that occurs from free **15** as this would be expected to eliminate the transient burst all together. The explanation for multiple turnovers in the burst phase must lie, therefore, in the two major chemical events that took place, namely the photolysis of **15** and the enzymatic oxidation of benzyl alcohol to benzaldehyde.

The photolysis mechanism of 2-nitrobenzyl ethers such as **15** is well-studied [10]. It has been proposed that nitroso- and benzyl-radicals are generated as one of the photolysis intermediates [13]. A plausible mechanism for the breakdown of **15** is shown in Scheme 3 [13]. Free radicals are able to inactivate yeast alcohol dehydrogenase (YADH) through reaction with active site cysteines and histidines, resulting in the loss of the active site zinc [18]. Additionally, a radical can interact with surface

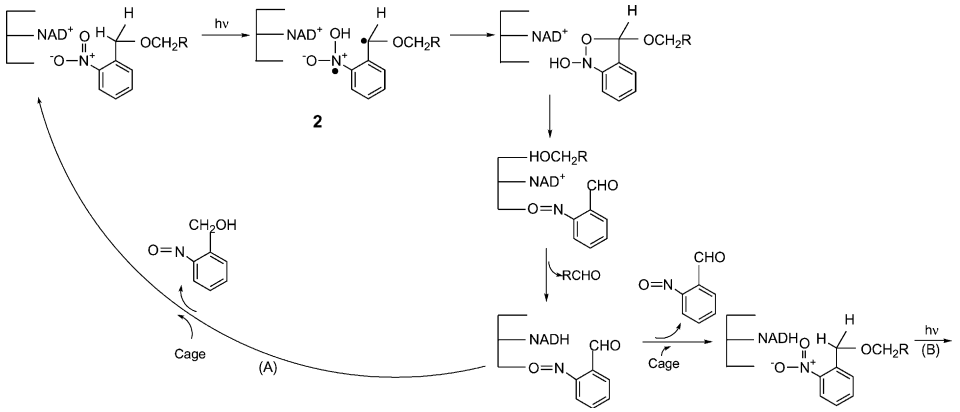

Scheme 3. Postulated mechanism for photolysis of caged reagents such as **15** [7], showing radical intermediates. Multiple turnovers could occur in the burst phase via oxidation of enzyme-bound NADH by the bound photoproduct, nitrosoaldehyde (A) or by photoinduced radicals formed from a second molecule of **15** (B).

cysteines in HLADH, enhancing protein denaturation [19]. However, the inactivation of YADH by the radical can be greatly reduced in the presence of NADH, which absorbs the radical and acts as a "radical protectant" for the enzyme [20]. In fact, it was found that NADH reacts readily with the nitroso radical and is re-oxidized to NAD^+ [20,21]. Since radical intermediates will be generated during the photolysis of **15**, some of the above side reactions between the radical intermediate and the enzyme/NADH may have taken place, namely, the inactivation of the enzyme (regardless of the mechanism) or the re-oxidation of NADH. Through control experiments, we found that laser irradiation on samples containing HLADH (20 μM) and NAD^+ (10 mM), with or without **15** (1 mM), did not affect the specific activity of the enzyme. This indicates that the enzyme was not damaged in the presence of radical intermediate due to the photolysis of **15**. Further laser irradiation on a sample containing ^{14}C-labeled benzyl alcohol (1 mM) and NAD (10 mM) did not produce detectable amount of product benzaldehyde while prolonged laser irradiation of a sample containing NADH (1 mM) and **15** (1 mM) resulted in a reduction of absorption at the λ_{max} of NADH (340 nm). These control experiments indicate that during the photolysis of **15**, there is no detectable radical damage on HLADH, benzyl alcohol or NAD^+, but that the amount of NADH is reduced. This suggests a re-oxidation of NADH to NAD^+ by a radical intermediate or aldehyde produced by photolysis (Scheme 3).

Mechanistic studies on HALDH-catalyzed benzyl alcohol oxidation have indicated that the two major rate limiting steps in the forward direction are the hydrogen-transfer reaction (23 s^{-1}) and NADH dissociation from the enzyme (5 s^{-1}) [22]. Scheme 3 shows a mechanism whereby enzyme-bound NADH formed from benzyl alcohol oxidation rebinds a second molecule of cage to form an intermediate analogous to **2**, but containing NADH instead of NAD^+. Oxidation of NADH by the

photoproduced radical would lead to enzyme-bound NAD^+, which could enter into a second productive reaction of cage (Scheme 3B). As an alternative, the nitrosoaldehyde photoproduct may stay bound to enzyme and facilitate the re-oxidation of NADH into NAD^+ (Scheme 3A). Essentially, the enzyme serves to provide a high local concentration of reactive radical or aldehyde that is capable of oxidizing enzyme-bound NADH back to NAD^+, thus bypassing the slow NADH-release step. The complexity of the processes in Scheme 3 could explain both the lack of an H/D KIE and the observed multiple turnovers in the fast phase (Fig. 3).

In closing, it is interesting to consider an alternative, though less likely explanation, for the multiple turnovers of **15** in the burst phase. This could arise from changes in the dynamic behavior of the protein that accompany the photochemistry, giving faster turnover with either free **15** or free benzyl alcohol. This idea, discussed by others in the context of "protein quakes" [23], is very interesting, implying that photo-excitation of a bound chromophore can change the dynamic properties of an enzyme-catalyzed reaction. The transfer of photo-excitation energy to the protein cannot be 100% efficient, and heat will be generated in the energy-transfer process. We monitored the reaction throughout the photolysis of **15** but did not detect any raise of the temperature. Therefore, this explanation is likely only if an unknown energy-transfer process can channel the photo-excitation energy into an enzyme-catalyzed reaction very efficiently or if heat is generated in a very local manner. We consider the participation of photolysis products in NADH oxidation to be the more likely cause of the observed multiple-turnovers, while noting the possibility that dissipation of photo-excitation energy may increase protein flexibility and, to some extent, enzyme turnover.

Acknowledgments

We thank Dr. H. Yang for his help in building the photolysis apparatus, as well as Prof. J. McCusker, Dr. N. Damrauer, and Dr. J. P. Kirby for their generous supply of the YAG laser.

References

[1] A. Fersht, Structure and Mechanism in Protein Science: A Guide to Enzyme Catalysis and Protein Folding, W.H. Freeman, New York, 1999.
[2] A. Kohen, J.P. Klinman, Chem. Biol. 6 (1999) 191.
[3] M.J. Knapp, J.P. Klinman, Eur. J. Biochem. 269 (2002) 113.
[4] M.J. Sutcliffe, N.S. Scrutton, Eur. J. Biochem. 269 (2002) 3096.
[5] E.C. Slater, Eur. J. Biochem. 166 (1987) 89.
[6] P.K. Agarwal, S.R. Billeter, P.T. Rajagopalan, S.J. Benkovic, S. Hammes-Schiffer, Proc. Natl. Acad. Sci. USA 99 (2002) 2794.
[7] M.J. Knapp, K. Rickert, J.P. Klinman, J. Am. Chem. Soc. 124 (2002) 3865.
[8] A. Kohen, R. Cannio, S. Bartolucci, J.P. Klinman, Nature 399 (1999) 496.
[9] S. Tsai, J.P. Klinman, Biochemistry 40 (2001) 2303.
[10] J.A. McCray, D.R. Trentham, Annu. Rev. Biophys. 18 (1989) 239.

[11] S. Ramaswamy, H. Eklnd, B.V. Plapp, Biochemistry 33 (1994) 5230.
[12] H. Eklund, B.V. Plapp, J.-P. Samama, C.-I. Branden, J. Biol. Chem. 257 (1982) 14349.
[13] H. Schupp, W.K. Wong, W. Schnabel, J. Photochem. 36 (1987) 85.
[14] H. Eckert, B. Forster, Angew. Chem. Int. Ed. Engl. 26 (1987) 894.
[15] R.D. Walkup, R.T. Cunnigham, Tetrahedron Lett. 28 (1987) 4019.
[16] D.L. Hughes, Org. React. 42 (1992) 335.
[17] U. Widmer, Synthesis 29 (1987) 568.
[18] S. Abelidis, J.S. Moore, A. Chakravarty, Int. J. Biol. Relat. Study Phys. Chem. Med. 52 (1987) 413.
[19] P. Waring, A. Sjaarda, Q.H. Lin, Biochem. Pharmacol. 49 (1995) 1195.
[20] L.A. Videla, M. Salim-Hanna, E.A. Lissi, Biochem. Pharmacol. 44 (1992) 235.
[21] H. Fujii, J. Koscielniak, K. Kakinuma, L.J. Berliner, Free Radic. Res. 21 (1994) 235.
[22] G.L. Shearer, K. Kim, K.M. Lee, C.K. Wang, B.V. Plapp, Bicohemistry 32 (1993) 11186.
[23] A. Ansari, J. Berendzen, S.F. Bowne, H. Frauenfelder, I.E.T. Iben, T.B. Sauke, E. Shyamsunder, R.D. Young, Proc. Natl. Acad. Sci. USA 82 (1985) 5000.